the flow rate is further increased, and after a narrow chaotic region, a cascade of reversed period-doubling bifurcations results in a $1^2$ limit cycle. The small oscillations circle the low-[$HBrO_2$] and low-[Ce(IV)] steady state. Another chaotic window is found at even higher flow rates and is followed by a $1^1$ periodicity. A chaotic attractor from this region is shown in Fig. 1*b* and is similar to experiment. Only isolated period-doubling bifurcations and periodic states were found at flow rates above the $1^1$ periodicity. Large-amplitude, regular $1^0$ oscillations appear above $k_f = 4.5 \times 10^{-4}\ s^{-1}$ and persist until the bifurcation to the high-flow-rate steady state is approached, and the situation again becomes complex.

The high flow rate[19] conditions are those of ref. 20: $A = [BrO_3^-] = 0.14$ M, $M = [MA] = 0.3$ M, $H = [H^+] = 0.26$ M and $C = [Ce]_{tot} = 0.001$ M. We used $\alpha = 333.3$ and $\beta = 0.2609$. There are regular, $1^0$ oscillations at $k_f = 2.02 \times 10^{-3}\ s^{-1}$. But several complex periodic and chaotic windows appear as $k_f$ is increased to $2.23 \times 10^{-3}\ s^{-1}$ where the oxidized, high-[$HBrO_2$] and high-[Ce(IV)] steady state has been reached. The complex periodic oscillations consist of a mixture of small-amplitude sinusoidal cycles around the high-[$HBrO_2$] and high-[Ce(IV)] steady state and large-amplitude relaxation oscillations. The ratio of small to large oscillations increases as the flow rate increases, with the main periodic states being $1^1$, $1^2$, $1^3$ and so on. Between any two of these periodic states there are more complex periodicities and chaos. The bifurcation diagram in Fig. 2*a* shows how the $1^4 1^5$ periodic window bifurcates through intermittency to chaos. The chaotic window contains several very complex periodic states and terminates in a $1^4 1^5 1^5$ limit cycle as the flow rate is increased. One of the strange attractors found in this region is shown in Fig. 2*b*. Small-amplitude, sinusoidal oscillations ($0^1$ periodicity) are found at $k_f = 2.22 \times 10^{-3}\ s^{-1}$, just before reaching the high-[$HBrO_2$] and high-[Ce(IV)] steady state.

These simulations have many features in common with experiments. The complexity at both high and low flow rates is embedded between small-amplitude, sinusoidal oscillations and large-amplitude, $1^0$, relaxation oscillations. The presence and appearance of the low-flow-rate $1^1$ and $1^2$ periodicities and their period-doubling bifurcation are as found experimentally. The sequence and appearance at high flow rates of various complex limit cycles with chaotic windows between them is also common to experiment and simulations.

Two main differences between experiment and simulations exist at low flow rates. First, the experimental bifurcation leading from sinusoidal to mixed-mode oscillations is probably a secondary-Hopf bifurcation rather than the sequence of period-doubling bifurcations found in simulations. Second, there is no chaos between the $1^1$ and the $1^0$ periodicities in the simulations, even though most of the available chaotic experimental results were obtained in this region. We did not search for a set of parameters that might remove these discrepancies.

Although the main features of BZ-CSTR chaos can be rationalized using only homogeneous kinetics as is done here, it is clear that mixing effects are important[11]. Chaos can be simulated by coupling mixing with a homogeneous model of the BZ kinetics that does not itself show chaos[11]. But the detailed agreement between simulations based on the mixing model and experiment is not as good as that between experiment and simulations based on the 11-variable homogeneous model[10]. We are now investigating the effect of mixing on chaotic homogeneous models such as that presented here. □

Received 13 May; accepted 27 November 1991.


1. Gleick, J. *Chaos. Making a New Science* (Viking, New York, 1987).
2. Hao, Bei-Lin *Chaos II* (*World Scientific*, Singapore, 1990).
3. Gray, P. & Scott, S. K. *Chemical Oscillations and Instabilities. Non-linear Chemical Kinetics* (Clarendon, Oxford, 1990).
4. Field, R. J. & Burger, M. (eds) *Oscillations and Traveling Waves in Chemical Systems* (Wiley, New York, 1985).
5. Belousov, B. P. in *Sbornik Referatov po Radiatsinnoi Meditsine* 145–147 (Medgiz, Moscow, 1958).
6. Zhabotinsky, A. M. *Biofizika* **9**, 306–311 (1964) (in Russian).
7. Field, R. J. & Noyes, R. M. *J. chem. Phys.* **60**, 1877–1884 (1974).
8. Luo, Y. & Epstein, I. R. *Adv. chem. Phys.* **79**, 269–299 (1990).
9. Györgyi, L. Turányi, T. & Field, R. J. *J. phys. Chem.* **94**, 7162–7170 (1990).
10. Györgyi, L., Rempe, S. & Field, R. J. *J. phys. Chem.* **95**, 3159–3165 (1991).
11. Györgyi, L. & Field, R. J. *J. chem. Phys.* **91**, 6131–6141 (1989).
12. Györgyi, L. & Field, R. J. *J. phys. Chem.* **95**, 6594–6602 (1991).
13. Field, R. J. & Försterling, H.-D. *J. phys. Chem.* **90**, 5400–5407.
14. Thikhonov, A. N. *Math. Sb.* **31**, 575–586 (1952) (in Russian).
15. Tyson, J. *J. phys. Chem.* **86**, 3006–3012 (1982).
16. Roux, J.-C., Simoyi, R. H. & Swinney, H. L. *Physica* D**8**, 257–266 (1983).
17. Coffman, K. G., McCormick, W. D., Noszticzius, Z., Simoyi, R. H. & Swinney, H. L. *J. chem. Phys.* **86**, 119–129 (1987).
18. Feigenbaum, M. J. *J. stat. Phys.* **19**, 25–52 (1978).
19. Schmitz, R. A., Graziani, K. R. & Hudson, J. L. *J. chem. Phys.* **67**, 3040–3044 (1977).
20. Hudson, J. L. & Mankin, J. C. *J. chem. Phys.* **74**, 6171–6177 (1981).


# Radiative forcing of climate from halocarbon-induced global stratospheric ozone loss


**V. Ramaswamy*, M. D. Schwarzkopf† & K. P. Shine‡**

* Atmospheric and Oceanic Sciences Program, Princeton University, Princeton, New Jersey 08542, USA
† NOAA/Geophysical Fluid Dynamics Laboratory, Princeton, New Jersey 08542, USA
‡ Department of Meteorology, University of Reading, Reading RG6 2AU, UK



**OBSERVATIONS from satellite and ground-based instruments[1–3] indicate that between 1979 and 1990 there have been statistically significant losses of ozone in the lower stratosphere of the middle to high latitudes in both hemispheres. Here we determine the radiative forcing of the surface–troposphere system[4–6] due to the observed decadal ozone losses, and compare it with that due to the increased concentrations of the other main radiatively active gases ($CO_2$, $CH_4$, $N_2O$ and chlorofluorocarbons) over the same time period. Our results indicate that a significant negative radiative forcing results from ozone losses in middle to high latitudes, in contrast to the positive forcing at all latitudes caused by the CFCs and other gases. As the anthropogenic emissions of CFCs and other halocarbons are thought to be largely responsible for the observed ozone depletions[1], our results suggest that the net decadal contribution of CFCs to the greenhouse climate forcing is substantially less than previously estimated.**


The radiative forcing of the surface-troposphere system is central to concerns about climate change due to trace gases[4]. The direct radiative forcing is defined[4,6] as the perturbation in the net radiative flux at the tropopause due to changes in concentrations of trace species, with water vapour changes and chemical interactions being excluded. This definition accounts for the rapid adjustment[7] of stratospheric temperatures to a new equilibrium in response to radiative perturbations, while all tropospheric parameters are held fixed. The radiative forcings are determined by assuming that there is no change in the dynamical heating of the stratosphere, using the fixed dynamical heating (FDH) concept[5,8–10]. New equilibrium temperatures are calculated for the stratosphere in response to the imposed radiative perturbations. The radiative fluxes calculated using the equilibrated stratospheric temperatures serve to determine the forcing[4].

Two zonally averaged FDH models with fixed cloud amounts[11] are used here: the Geophysical Fluid Dynamics Laboratory (GFDL) 40-level model[9,12] (latitude range 4.5 to 76.5° in 9° steps), and the 19-level University of Reading model[13,14] (latitude range: 0 to 80° in 10° steps). Both models use a 10-$cm^{-1}$ narrow-band algorithm[15] to calculate longwave radiation and assume cloud emissivities to be unity, but they have different solar radiation schemes, and different initial temperature, moisture and ozone climatologies. The GFDL results are for perturbations in January, April, July and October; the Reading results are for January and July in the Northern Hemisphere.

TABLE 1 Net radiative forcing of the surface-troposphere system

| Latitude | Non-ozone gases | | Ozone | | |
|---|---|---|---|---|---|
| | CFCs ($W m^{-2}$) | All ($W m^{-2}$) | Solar radiative forcing ($W m^{-2}$) | Net radiative forcing without stratospheric temperature change ($W m^{-2}$) | Net radiative forcing with stratospheric temperature change ($W m^{-2}$) |
| 90-60° N | 0.05 (0.05) | 0.30 (0.33) | 0.12 (0.07) | 0.04 (−0.06) | −0.15 (−0.18) |
| 60-30° N | 0.09 (0.08) | 0.41 (0.43) | 0.16 (0.11) | 0.09 (0.01) | −0.13 (−0.15) |
| 30-10° N | 0.13 (0.14) | 0.54 (0.53) | 0.07 (0.08) | 0.06 (0.04) | −0.04 (−0.04) |
| 10° N-10° S | 0.11(0.12) | 0.50 (0.51) | −0.01 (0.02) | −0.01 (0.01) | 0.0 (−0.01) |
| 10-30° S | 0.12 | 0.53 | 0.0 | 0.0 | 0.0 |
| 30-60° S | 0.10 | 0.43 | 0.19 | 0.11 | −0.11 |
| 60-90° S | 0.05 | 0.28 | 0.17 | 0.03 | −0.30 |
| Northern Hemisphere | 0.10 (0.11) | 0.45 (0.47) | 0.10 (0.08) | 0.06 (0.01) | −0.08 (−0.09) |
| Southern Hemisphere | 0.10 | 0.46 | 0.10 | 0.05 | −0.08 |
| Global | 0.10 | 0.45 | 0.10 | 0.06 | −0.08 |

Net radiative (solar plus longwave) forcing due to the 1979-90 increases in CFCs and in all non-ozone gases, and that due to the observed stratospheric ozone losses. The net radiative forcing is obtained with the stratosphere in equilibrium in the presence of a fixed dynamical heating. The GFDL model results are averages over the four mid-season months, whereas the Reading model results (in parentheses) are averages over January and July only. Positive values denote gain of radiative energy.

The increases in the concentrations of the radiatively active, non-ozone gases between 1979 and 1990 are taken from ref. 1 (ch. 8). The changes in column ozone at each latitude over the same time period follow TOMS (total ozone mapping spectrometer) data[2]. On the basis of the observed profiles[1,3,16], we assume that the depletions occur in the lower stratosphere, with an equal percentage change applied in each model layer between the tropopause and ~7 km above it (the vertical profile of the loss assumed here differs slightly from ref. 1). The location of the tropopause in the models is somewhat arbitrary and is used here to infer general implications for the surface-troposphere forcing. The tropopause in the GFDL model varies linearly with latitude from 100 mbar at the Equator to 270 mbar at 76.5°. In the Reading model, it is assumed to be at 96 mbar from 0 to 30° N (40° N in July), at 180 mbar from 30 to 50° N (60° N in July) and at 292 mbar thereafter.

The decadal increases in trace gases other than ozone induce a latitudinally dependent increase in the surface-troposphere forcing (Fig. 1 and Table 1). Loss of ozone in the lower stratosphere induces three distinct radiative effects[5,6]: (1) more solar radiation reaches the surface-troposphere system (Table 1); (2) in the absence of stratospheric temperature changes, less longwave radiation is emitted into the surface-troposphere system and the ensuing forcing (Table 1) is lower than it would be for the solar effect alone; and (3) the *in situ* solar heating is reduced and there is a change in the convergence of longwave radiation in the lower stratosphere. Because the lower stratosphere is sensitive to radiative perturbations[9,10,17,18], this results, in the absence of any compensatory dynamical heating, in a decrease of temperatures at these altitudes. This, in turn, further reduces longwave emission from the stratosphere into the troposphere by an amount depending on the decrease in stratospheric temperature. The result in the middle to higher latitudes is an enhancement of the longwave effect over the solar, leading to a net negative radiative forcing (Table 1). Within the surface-troposphere system, the (positive) solar effect is 'felt' primarily at the surface, whereas the (negative) longwave effect is 'felt' primarily in the troposphere[1,5].

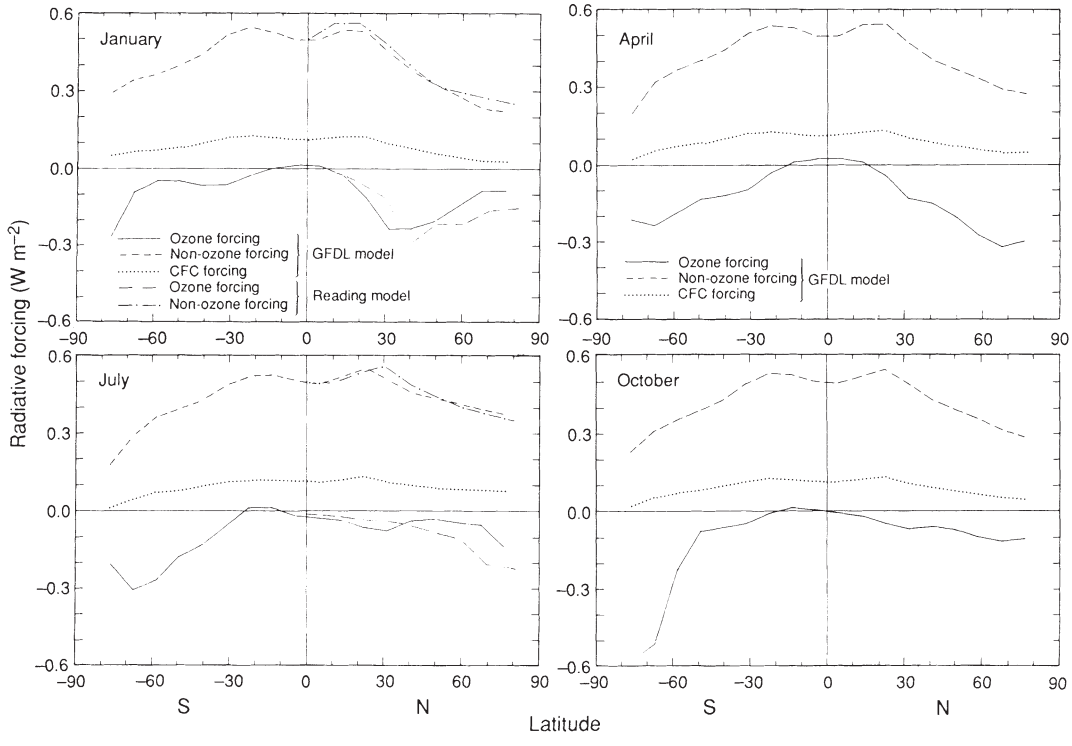


FIG. 1 Latitudinal dependence of the surface-troposphere radiative forcing due to the 1979-90 increases in (1) CFCs alone and (2) all the non-ozone gases ($CO_2$, $CH_4$, $N_2O$ and CFCs), and that due to losses of ozone in the lower stratosphere. Results from the Reading model are for Northern Hemisphere January and July perturbations only, whereas the GFDL results are for perturbations corresponding to each of the four mid-season months (January, April, July and October). All the results were obtained by assuming stratospheric equilibrium in the presence of a fixed dynamical heating.

The resultant net ozone radiative forcing is compared with that due to the other radiatively active gases in Fig. 1 and Table 1. The ozone forcing depends on the amount of ozone loss[2] and insolation and thus on the season and latitude. Differences between the models arise because of different initial atmospheric profiles and different solar radiation algorithms. Poleward of 30°, the magnitude of the (negative) ozone forcings becomes comparable to and can even exceed the (positive) CFC forcing. At these latitudes, the magnitude of the ozone forcing can also be a considerable fraction of the (positive) non-ozone gas forcing. When globally and annually averaged (Table 1), the ozone forcing results in a substantial offset (~80%) of the decadal CFC greenhouse forcing, and a reduction of ~18% in the decadal greenhouse gas forcing.

There is strong evidence that the Antarctic ozone losses are primarily due to chlorine- and bromine-containing chemicals (halocarbons)[1]. Evidence also suggests that a large part of the observed global loss in lower stratospheric ozone results from emissions of CFCs and other halocarbons[1]. If this is so, then the net planetary greenhouse effect due to the halocarbons is the sum of their direct radiative effect and the indirect chemical effect by means of ozone depletion. Our calculations indicate that the chemical effects, in the global mean, substantially reduce the direct radiative effects of the CFCs. But the offset is not uniform with latitude (Fig. 1; Table 1); the total (CFCs plus ozone) forcing is positive at low latitudes owing to increases in CFCs, and negative at high latitudes owing to ozone losses. It would be difficult to decompose the observed ozone depletion into that due to individual halocarbons. Our calculations can only indicate the ozone-depleting effect of all halocarbons against the greenhouse effect of the CFCs.

Uncertainties in our calculations include cloud[1] and moisture distributions within the troposphere and the ozone trend[3] below ~17 km. The radiative effects of stratospheric ozone are sensitive to the altitude profile of ozone loss[19]. Our calculations show that the magnitude of the ozone forcing would be reduced if the principal ozone losses were concentrated at altitudes higher than assumed here. For example, if the column ozone loss[2] were distributed on an equal percentage basis throughout the stratosphere, an assumption in which the principal losses occur at altitudes higher than observations indicate[3], the GFDL and Reading models indicate a global mean forcing of −0.01 and −0.04 W m$^{-2}$ respectively. The ozone forcing could even become positive if the losses were confined to the upper stratosphere[20]. In contrast to the stratospheric losses, a different set of factors[1] can cause an increase of ozone in the troposphere, yielding a positive forcing[5]. Because data are sparse the global trends due to this effect cannot be quantified at present[1]. The need for accurate observations of changes in the total column and the vertical profile of ozone cannot be overemphasized.

We cannot yet ascertain whether the atmospheric dynamical response[21] would enhance or reduce the ozone-induced radiative cooling tendency in the lower stratosphere. But general circulation model (GCM) studies of uniform perturbations of column ozone indicate that, unless the depletions are large (>50%), there is no significant change in the stratospheric dynamical activity[21]. The lower-stratospheric temperature response in these GCM studies is one of cooling and, in the middle and high latitudes, it is at least 70% of the response in the absence of dynamical changes[9,10]. For an assumed scenario of global ozone changes and for the Antarctic springtime depletions, the GCM and FDH temperature responses are similar[10,22,23].

Observations for the periods 1973–87 (ref. 24) and 1958–89 (ref. 25) indicate a mean cooling trend for the global lower stratosphere (50–100 mbar). The temperature changes per decade estimated by two different linear-trend analyses in refs 24 and 25 are −0.34 ± 0.38 K and −0.39 ± 0.09 K, respectively, for the Northern Hemisphere, and −0.90 ± 0.67 K and −0.45 ± 0.15 K, respectively, for the Southern Hemisphere. The models give coolings per decade in the 50–100-mbar layer of −0.47 K (GFDL; global) and −0.64 K (Reading; Northern Hemisphere), and occur mainly because of the ozone losses. Although the model results are within or at the higher end of the fairly large uncertainty limits in the observed trends, physical factors other than ozone losses[21,26] (changes in tropospheric state, volcanic aerosols and so on) may also be contributing to the trends. Although we have investigated the radiative forcing of the surface–troposphere system, models of latitudinal changes in surface temperature and in the atmospheric general circulation require additional considerations (for example, the three-dimensional distribution of radiative perturbations[6,27], and dynamical feedbacks) and can be resolved only through GCM studies. □

Received 18 November 1991; accepted 7 January 1992.


1. WMO/UNEP *Scientific Assessment of Ozone Depletion: 1991* (WMO, Geneva, in the press).
2. Stolarski, R. S., Bloomfield, P., McPeters, R. D. & Herman, J. R. *Geophys. Res. Lett.* **18,** 1015–1018 (1991).
3. McCormick, M. P., Veiga, R. E. & Chu, W. P. *Geophys. Res. Lett.* (in the press).
4. Shine, K. P., Derwent, R. G., Wuebbles, D. J. & Morcrette, J.-J. in *Climate Change: The IPCC Scientific Assessment* (eds Houghton, J. T. *et al.*) 41–68 (Cambridge University Press, 1990).
5. Ramanathan, V. & Dickinson, R. E. *J. atmos. Sci.* **36,** 1084–1104 (1979).
6. Ramanathan, V. *et al. Rev. Geophys.* **25,** 1441–1482 (1987).
7. Hansen, J. *et al. Science* **213,** 957–966 (1981).
8. Fels, S. B. & Kaplan, L. D. *J. atmos. Sci.* **33,** 779–789 (1975).
9. Fels, S. B., Mahlman, J. D., Schwarzkopf, M. D. & Sinclair, R. W. *J. atmos. Sci.* **37,** 2265–2297 (1980).
10. Kiehl, J. T. & Boville, B. A. *J. atmos. Sci.* **45,** 1798–1817 (1988).
11. London, J. College of Engineering, New York Univ. *Rep. contract* AF19(122)-165 (NTIS No. 117227) (1957).
12. Mahlman, J. D. & Umscheid, L. in *Dynamics of the Middle Atmosphere* (eds Holton, J. R. & Matsuno, T.) 501–525 (Terrapub, Tokyo, 1984).
13. Shine, K. P. *J. atmos. Sci.* **48,** 1513–1518 (1991).
14. Slingo, A. & Schrecker, H. M. *Q. Jl R. met. Soc.* **108,** 407–426 (1982).
15. Malkmus, W. *J. opt. Soc. Am.* **57,** 323–329 (1967).
16. Solomon, S. *et al. Nature* **321,** 755–758 (1986).
17. Kiehl, J. T. & Solomon, S. *J. atmos. Sci.* **43,** 1525–1534 (1986).
18. Shine, K. P. *Q. Jl R. met. Soc.* **113,** 603–633 (1987).
19. Lacis, A. A., Wuebbles, D. J. & Logan, J. A. *J. geophys. Res.* **95,** 9971–9981 (1990).
20. Ramanathan, V., Cicerone, R. J., Singh, H. B. & Kiehl, J. T. *J. geophys. Res.* **90,** 5547–5566 (1985).
21. WMO *Report of the International Ozone Trends Panel 1988*, ch. 6, *Global Ozone Research and Monitoring Project Rep.* No. 18 (1989).
22. Kiehl, J. T., Boville, B. A. & Briegleb, B. P. *Nature* **332,** 501–504 (1988).
23. Shine, K. P. *Geophys. Res. Lett.* **13,** 1331–1334 (1986).
24. Angell, J. K. *J. Clim.* **1,** 1296–1313 (1988).
25. Oort, A. & Liu, H. *J. Clim.* (in the press).
26. WMO *Scientific Assessment of Stratospheric Ozone: 1989*, ch. 1, *Global Ozone Research and Monitoring Project Rep.* No. 20, (1990).
27. Wang, W.-C., Dudek, M. P., Liang, X.-Z. & Kiehl, J. T. *Nature* **350,** 573–577 (1991).


ACKNOWLEDGEMENTS. K.P.S. acknowledges partial support from the UK Joint Environmental Program of National Power and Power Generation. We thank J. T. Kiehl, J. D. Mahlman, S. Manabe and V. Ramanathan for helpful discussions.

# Upwelling and productivity changes inferred from a temperature record in the central equatorial Pacific

**M. W. Lyle*, F. G. Prahl† & M. A. Sparrow†**

* Borehole Research Group, Lamont-Doherty Geological Observatory, Palisades, New York 10964, USA
† College of Oceanography, Oregon State University, Corvallis, Oregon 97331-5503, USA

**A SERIES of $C_{37-39}$ alkenones synthesized by prymnesiophyte algae is commonly preserved in marine sediments, and can be used for estimating past sea surface temperatures (SSTs)[1,2]. Here we present an alkenone analysis of sediments taken from the central equatorial Pacific Ocean (core W8402A-14GC; 0° 57′ N, 138° 57′ W) which shows that SST varied slightly (<2 °C) but coherently with Milankovitch insolation cycles over the past 250 kyr. The in-phase response of the SST to the precessional component of insolation indicates that this part of the SST time series may be driven by changes in local trade-wind strength, and the longer 100-kyr eccentricity component indicates a response to basin-wide South Pacific winds. Using a simple heat-balance**